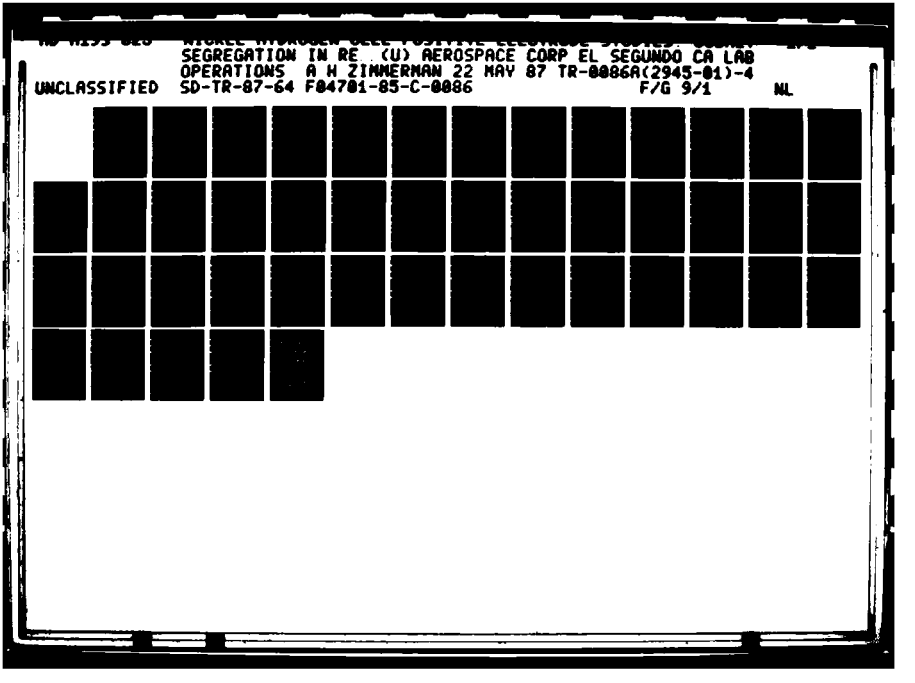
SEGREGATION IN RE (U) AEROSPACE CORP EL SEGUNDO CA LAB
OPERATIONS A H ZIMMERMAN 22 MAY 87 TR-0086A(2945-01)-4
UNCLASSIFIED SD-TR-87-64 F04701-85-C-0086 F/G 9/1 NL

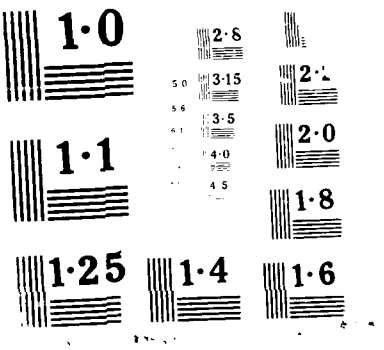
1·0
1·1
1·25
1·4
1·6
1·8
2·0
2·5
3·15
3·5
4·0
4·5
5·0
5·6

REPORT SD-TR-87-64

AD-A193 025

Nickel Hydrogen Cell Positive-Electrode Studies: Cobalt Segregation in Reducing Environments

A. H. ZIMMERMAN
Laboratory Operations
The Aerospace Corporation
El Segundo, CA 90245-4691

22 May 1987

Prepared for

SPACE DIVISION
AIR FORCE SYSTEMS COMMAND
Los Angeles Air Force Base
P.O. Box 92960, Worldway Postal Center
Los Angeles, CA 90009-2960

This report was submitted by The Aerospace Corporation, El Segundo, CA 90245, under Contract No. F04701-85-C-0086-P00016 with the Space Division, P.O. Box 92960, Worldway Postal Center, Los Angeles, CA 90009-2960. It was reviewed and approved for The Aerospace Corporation by S. Feuerstein, Director, Chemistry and Physics Laboratory.

Lt Thomas Wetterstroem, CWASB was the project officer for the Mission-Oriented Investigation and Experimentation (MOIE) Program.

This report has been reviewed by the Public Affairs Office (PAS) and is releasable to the National Technical Information Service (NTIS). At NTIS, it will be available to the general public, including foreign nationals.

This technical report has been reviewed and is approved for publication. Publication of this report does not constitute Air Force approval of the report's findings or conclusions. It is published only for the exchange and stimulation of ideas.

Thomas Wetterstroem

THOMAS WETTERSTROEM, Lt, USAF
MOIE Project Officer
SD/CWASB

Raymond M Leong

RAYMOND M. LEONG, Major, USAF
Deputy Director, AFSTC West Coast Office
AFSTC/WCO OL-AB

UNCLASSIFIED

SECURITY CLASSIFICATION OF THIS PAGE

REPORT DOCUMENTATION PAGE

1a REPORT SECURITY CLASSIFICATION Unclassified	1b. RESTRICTIVE MARKINGS
2a SECURITY CLASSIFICATION AUTHORITY	3. DISTRIBUTION / AVAILABILITY OF REPORT Approved for public release;
2b DECLASSIFICATION / DOWNGRADING SCHEDULE	Distribution unlimited.
4. PERFORMING ORGANIZATION REPORT NUMBER(S) TR-0086A(2945-01)-4	5. MONITORING ORGANIZATION REPORT NUMBER(S) SD-TR-87-64
6a. NAME OF PERFORMING ORGANIZATION The Aerospace Corporation Laboratory Operations 6b. OFFICE SYMBOL (If applicable)	7a. NAME OF MONITORING ORGANIZATION Space Division
6c. ADDRESS (City, State, and ZIP Code) El Segundo, CA 90245	7b. ADDRESS (City, State, and ZIP Code) Los Angeles Air Force Base Los Angeles, CA 90009-2960
8a. NAME OF FUNDING / SPONSORING ORGANIZATION 8b. OFFICE SYMBOL (If applicable)	9 PROCUREMENT INSTRUMENT IDENTIFICATION NUMBER F04701-85-C-0086-P00016
8c. ADDRESS (City, State, and ZIP Code)	10 SOURCE OF FUNDING NUMBERS PROGRAM ELEMENT NO. / PROJECT NO. / TASK NO. / WORK UNIT ACCESSION NO.

11 TITLE (Include Security Classification)
Nickel Hydrogen Cell Positive-Electrode Studies:
Cobalt Segregation in Reducing Environment

12 PERSONAL AUTHOR(S)
Zimmerman, Albert H.

13a. TYPE OF REPORT	13b TIME COVERED FROM ____ TO ____	14. DATE OF REPORT (Year, Month, Day)	15 PAGE COUNT
		1987 May 22	44

16 SUPPLEMENTARY NOTATION

17 COSATI CODES			18 SUBJECT TERMS (Continue on reverse if necessary and identify by block number)
FIELD	GROUP	SUB-GROUP	Batteries, High energy density, Fuel cells, Spacecraft power requirements

19. ABSTRACT (Continue on reverse if necessary and identify by block number)

Nickel electrodes from nickel hydrogen battery cells that had exhibited anomalously low capacities have been tested. Electrode characterization tests showed that changes had occurred in the electrode active material to increase the charge and discharge voltages. The increased charge voltages resulted in a decrease in charge efficiency. These changes apparently resulted from storage of the cell at low voltage with excess hydrogen present in the cell. Chemical and physical analyses indicated that cobalt, a 10% additive in the nickel electrode active material, had undergone segregation from the active material to form a cobalt-rich compound that is not normally present in the electrodes. This chemical change is felt to be largely responsible for the changes in electrode performance. A model for the processes causing cobalt segregation is described, and test results are presented to support the model.

20 DISTRIBUTION / AVAILABILITY OF ABSTRACT	21. ABSTRACT SECURITY CLASSIFICATION
☒ UNCLASSIFIED/UNLIMITED ☒ SAME AS RPT ☐ DTIC USERS	
22a NAME OF RESPONSIBLE INDIVIDUAL	22b TELEPHONE (Include Area Code) / 22c OFFICE SYMBOL

DD FORM 1473, 84 MAR 83 APR edition may be used until exhausted. All other editions are obsolete.

SECURITY CLASSIFICATION OF THIS PAGE

UNCLASSIFIED

CONTENTS

TABLES

FIGURES

I. INTRODUCTION

The nickel hydrogen battery cell provides a chemical environment that in some respects is quite unique from the environments within nickel cadmium or other alkaline battery cells. For example, the capability of the hydrogen electrode to catalyze hydrogen or oxygen reactions provides the cell with relative immunity from much of the stress associated with overcharge or overdischarge in other types of cells. However, the presence of hydrogen gas in intimate contact with all cell components can also provide a strongly reducing chemical environment in situations where the cell voltage is allowed to fall to low values with hydrogen present. The reducing environment that is achieved at the nickel electrode in this situation is unlike that which exists in any other battery cells. Under such conditions, it is possible that chemical or electrochemical reactions that are normally thought not to occur in battery cells can occur with appreciable rates in nickel hydrogen cells. Such reactions, which may either change cell operating characteristics or irreversibly degrade cell performance, are the subject of this study.

One of the first indications that some unique changes can occur in nickel hydrogen cells was provided by the empirical observation that cells that had been stored in a low voltage or shorted-down state often exhibited a loss of capacity that was difficult to recover during subsequent cycling. Additional observations by users of nickel hydrogen cells indicated that capacity fading was a problem only when excess hydrogen was present during the shorted-down storage. The loss of capacity was not readily recoverable, although some restoration of capacity was obtained by combinations of reconditioning and hundreds of LEO (low-earth orbit) cycles at a high DOD (depth of discharge). After several periods of storage for some cells, capacity losses of 20 to 30% were observed. At this level of degradation, several cells were disassembled. Nickel electrodes from one of these cells (S/N 114) were obtained for analysis to determine the most likely cause or causes for the degraded capacity.

This report presents the results of the analysis of the performance and properties of nickel electrodes from the S/N 114 cell. The focus of this study

is on electrode characteristics that appear to be different from the characteristics of an unused electrode from the same production lot (Lot 1008). Such differences in electrode characteristics are expected to arise either from the cycling seen by the cell relative to the unused electrodes or from other degradation processes that could have caused the fading in capacity. The effects of the electrode cycling in the cell could have been eliminated by comparison to cycled electrodes that did not exhibit a degraded capacity; however, such electrodes were not available. The tests that were done on the electrode samples were done both on the electrodes and on samples of active material and other electrode constituents that were either physically or chemically isolated from the nickel electrodes. These tests included charge/discharge cycling, I/V (current/voltage) measurement during overcharge, I/V measurement for discharged electrodes, charge efficiency measurements, effects of cycling, impedance characteristics, bulk chemical analyses, x-ray diffraction, ESCA (electron spectroscopy for chemical analysis), SEM (scanning electron microscopy), and EVS (electrochemical voltage spectroscopy).

II. ANALYSIS OF NICKEL ELECTRODE PROPERTIES AND PERFORMANCE

A. ELECTRODE CHARACTERIZATION

1. ELECTRICAL PERFORMANCE

The first tests involved measuring the charge/discharge voltages and capacities of the nickel electrodes designated as Lot 1008 and S/N 114. The S/N 114 nickel hydrogen cell had exhibited a degraded capacity using a 16-h C/10 charge. (The C rate will discharge the nameplate cell capacity in 1 hour.) Electrodes were charged at C/10 for periods of 12, 16, 24, and 36 h. Figures 1 and 2 indicate the discharge voltages following these charge periods for the Lot 1008 and S/N 114 electrodes, respectively. Prior to each charge/discharge cycle, each electrode sample was subjected to a conditioning cycle of a 24-h C/10 charge, followed by discharge at C/2 to 0.2 V, C/20 to -0.4 V, and C/100 to -0.5 V. All voltages were measured relative to a Hg/HgO reference electrode, which gives voltages close to 1.0 V lower than for the nickel hydrogen cell. All electrode samples were operated in a closed plastic cell, flooded with 31% potassium hydroxide electrolyte, and controlled at a temperature of 23°C. Typical electrode samples tested were 1 cm square. The C rate was assumed to be 20 mA/cm^2 for all electrodes.

The discharge voltages in Figs. 1 and 2 clearly show a two-step discharge behavior that has been associated with discharge of β-NiOOH that is formed initially during charge, followed by discharge of γ-NiOOH at somewhat lower voltages (Ref.1). The γ -NiOOH phase is formed during overcharge, and can lead to a significantly higher discharge capacity following extended overcharge. The S/N 114 samples appear to form the γ-NiOOH phase much more readily than do the Lot 1008 samples. Furthermore, the S/N 114 electrodes appear to discharge at voltages that are significantly higher than the Lot 1008 electrodes for both the β- and γ-NiOOH phases. This suggests that all of the active material in the S/N 114 electrodes has somehow been altered to have a higher characteristic voltage. The charge voltages for 36 h of a C/10 charge are indicated in Fig. 3 for the two kinds of electrodes. Again, the charge voltages clearly show a higher characteristic voltage for the S/N 114

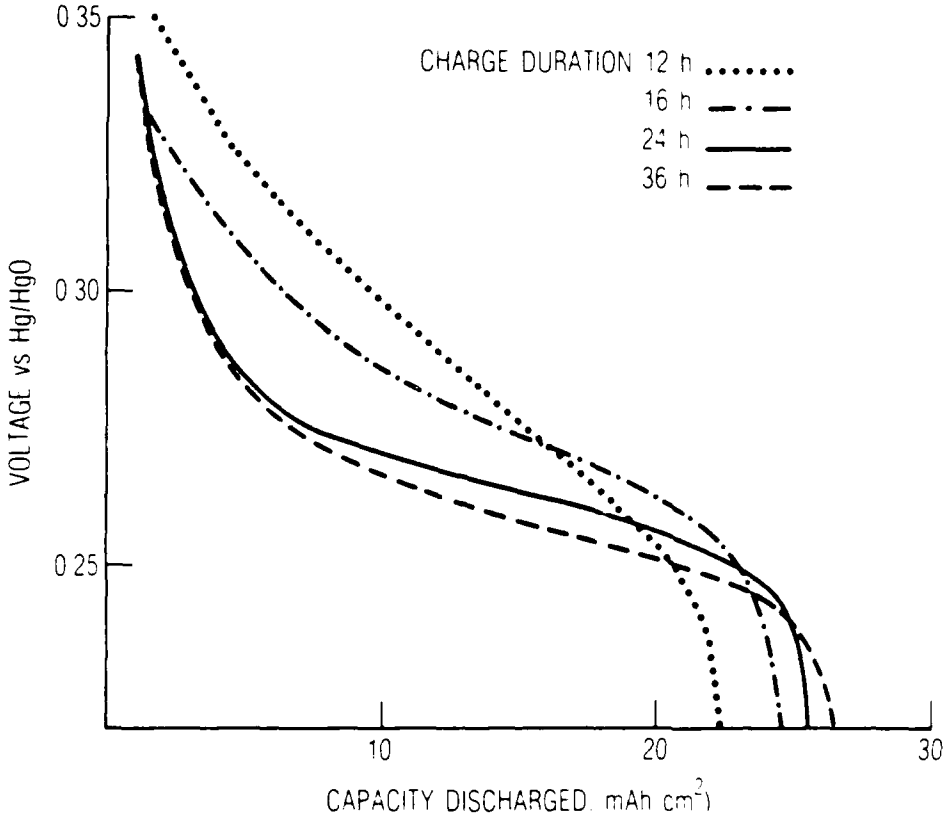

Fig. 1. Lot 1008 Ni Electrode Discharge (C/10) Following C/10 Charge

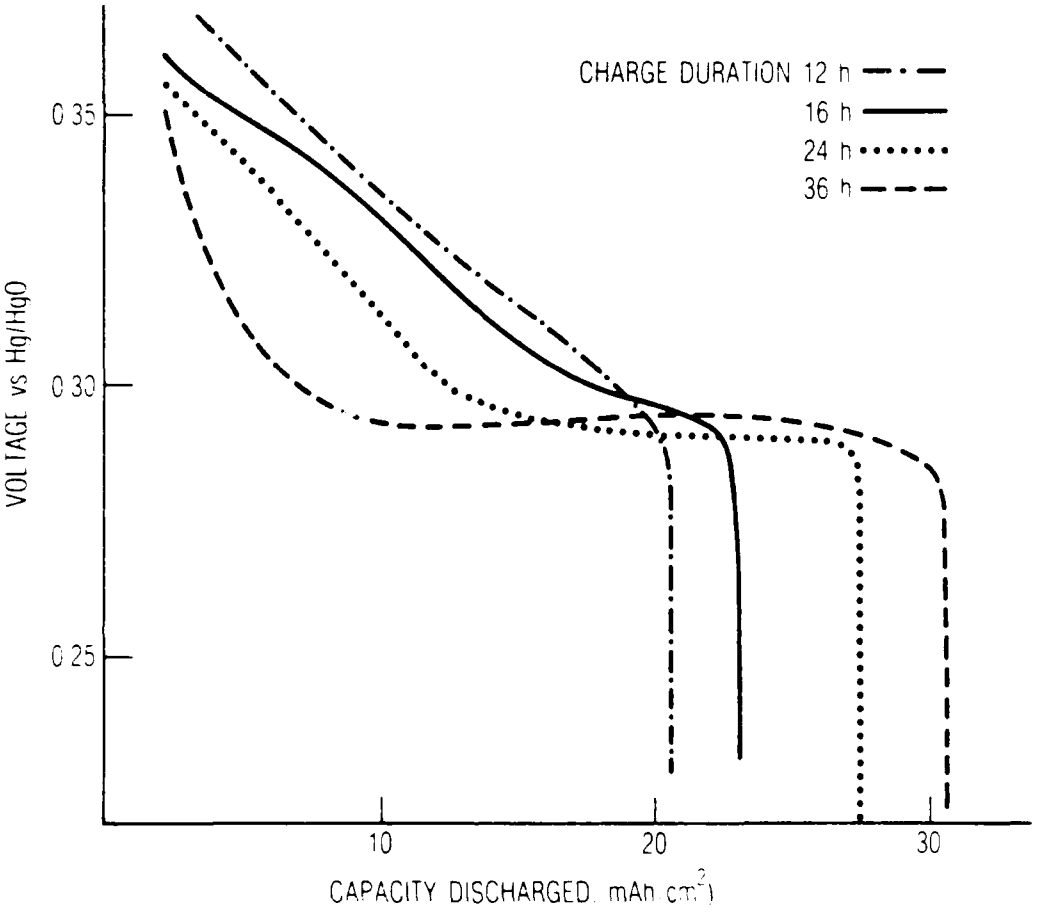

Fig. 2. S/N 114 Ni Electrode Discharge (C/10) Following C/10 Charge

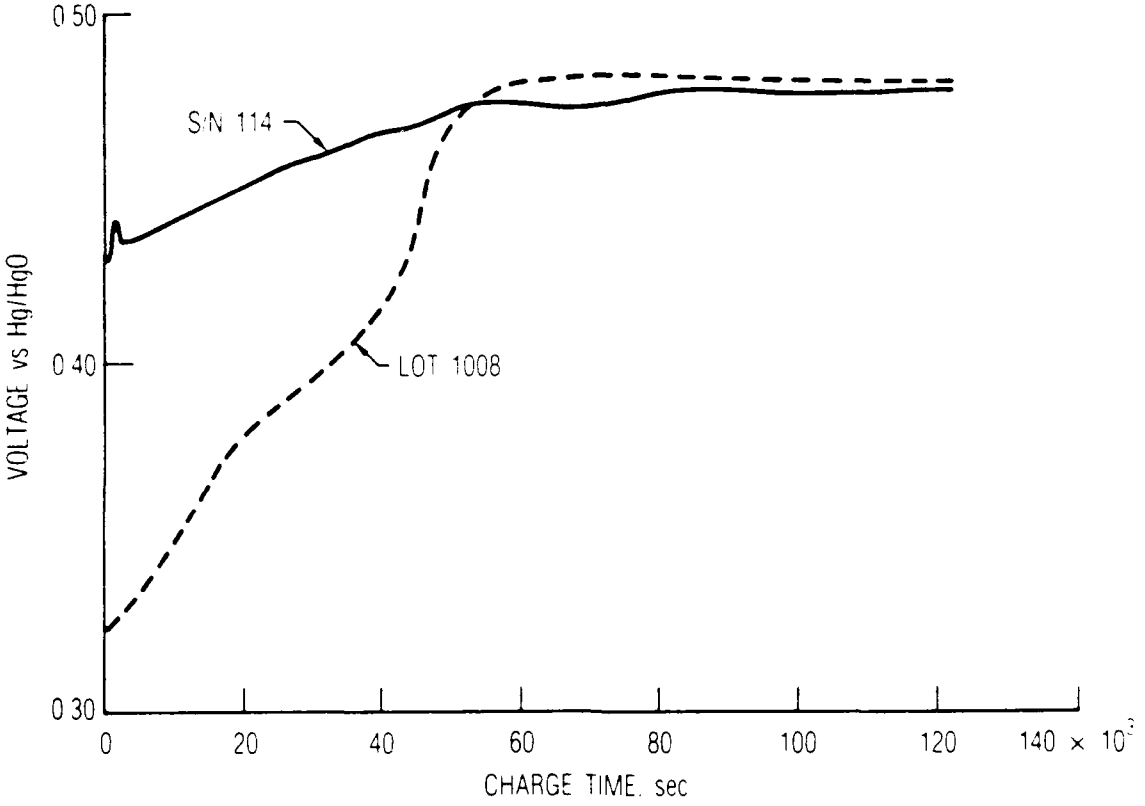

Fig. 3. Charge Voltage at C/10 for Ni Electrodes

electrode. Since Fig. 3 indicates that the oxygen evolution voltages of the two electrodes are not widely different, it is expected that the S/N 114 electrode that is charging at the higher voltage is likely to begin to generate oxygen sooner during charge than does the Lot 1008 electrode. This should result in a lower charge efficiency for the S/N 114 electrode for the first 10 to 14 h of the charge period. Table I indicates the capacities discharged at the C/10 rate for differing charge times. Since residual capacities were similar for all the charge times for a given electrode, the results of Table I confirm that the charge efficiency for the first 10 to 14 h of C/10 charging is lower for the S/N 114 electrode.

Table I. Electrode Capacities for Various C/10 Charge Times

Charge Time	Lot 1008 capacity	S/N 114 capacity
12 h	22.64 mAh	20.77 mAh
16	24.72	23.15
24	25.84	27.49
36	26.80	30.74

The I/V characteristics for the electrodes were measured in the overcharge or oxygen evolution region following a 36-h charge period at a C/10 rate. These measurements involved varying the overcharge current in steps, going from C/100 up to C/2. The electrode was allowed to remain at each current until a stable voltage reading was obtained (less than 0.1 mV change in 5 min). The measured I/V characteristics are presented in Fig. 4 for the two electrodes. The results in Fig.4 have been corrected for IR (voltage) drop in the solution between the nickel electrode and the reference electrode, which was determined by measuring the instantaneous voltage response to a small current step. The two kinds of electrodes in Fig. 4 do not show large differences in their I/V characteristics for oxygen evolution.

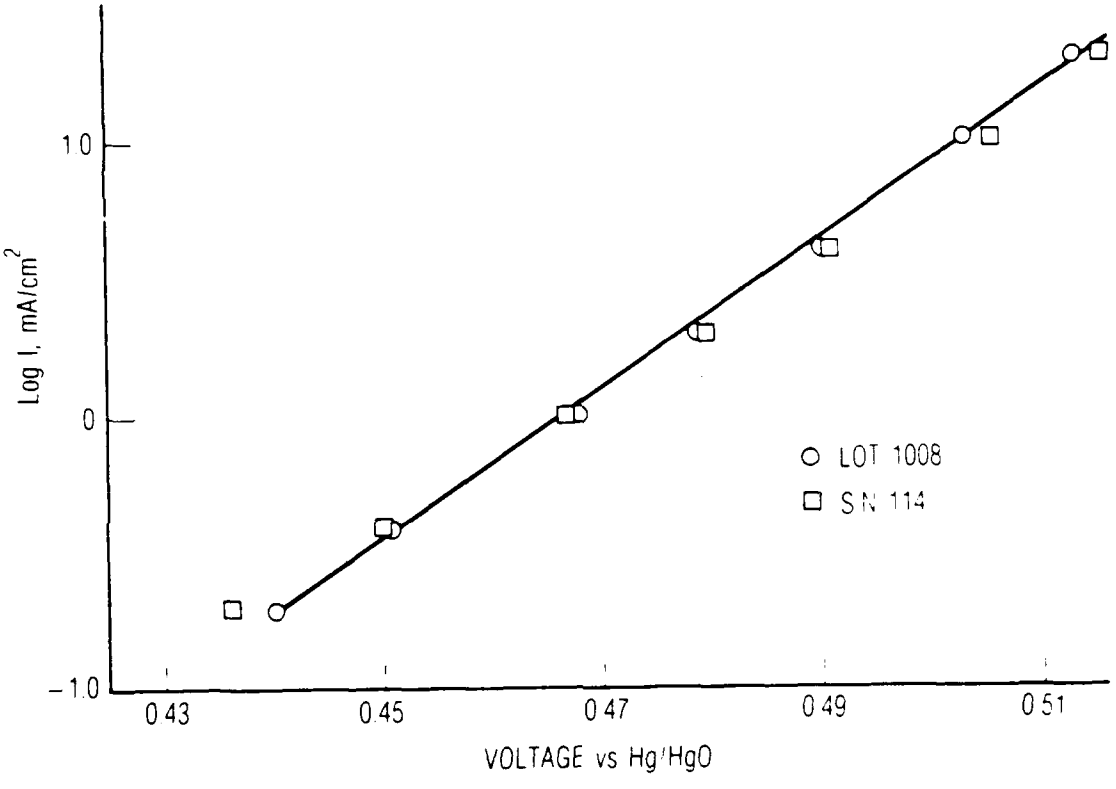

Fig. 4. I/V Behavior During Steady-State Oxygen Evolution for Ni Electrodes

The results of Figs. 3 and 4 may be combined to determine the charge efficiency as a function of time during the indicated C/10 charge. This is determined by recognizing that the charge efficiency at time t is given by

$$N(t) = 1 - [I_o/I(t)] \quad (1)$$

where I_o is the partial current going into oxygen evolution at time t, and I(t) is the total charge current at time t. The partial current I_o may be determined from the voltage in Fig. 3 using the I/V lines in Fig. 4. The assumption in this calculation is that the oxygen I/V behavior prior to overcharge is the same as that after extended overcharge. This assumption was eliminated by allowing for an offset in the oxygen evolution overpotential prior to voltage rollover. The magnitude of the voltage offset was adjusted so that the measured total capacity discharged after the charge period matched the capacity calculated by integrating Eq. (1). It was interesting to note that the offset in the oxygen evolution voltage had about the same amplitude as the rollover seen in the charge voltage for both electrodes. This offset in oxygen evolution voltage has been previously noted (Ref.2).

The charge efficiencies that were calculated are indicated in Fig. 5, and clearly show the lower charge efficiency for the S/N 114 electrode during the early portion of the charge period. The tailing off of the charge efficiency at long charge times is likely to be due to charging to the γ-NiOOH phase, a process that is known to have a low efficiency (Ref.1), particularly at charge rates as low as C/10. Several reasons may account for the lower charge efficiency of the S/N 114 electrodes. First, the cycling that these electrodes have experienced in the nickel hydrogen cell can degrade charge efficiency somewhat. The charge efficiency differences indicated in Table I and Fig. 5 for the two electrode types appear to be more than can be accounted for by normal performance changes arising from a moderate number of charge/discharge cycles, although this is likely to be a contributing factor. The second factor is the process that has caused the unusual increase in characteristic discharge voltage, which has, by raising the charge voltage, also decreased charge efficiency.

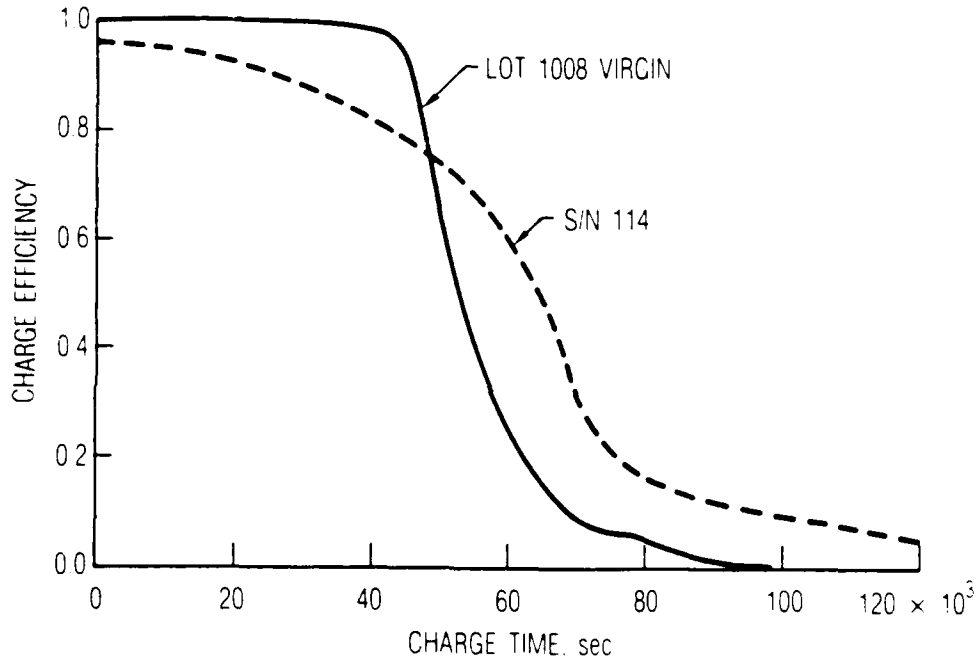

Fig. 5. Change Efficiencies Calculated Using Eq. (1) for the C/10 Charge Profiles of Fig. 3

The electrode behavior in these tests appears to parallel the nickel hydrogen cell behavior in many respects, in particular the high discharge voltages and lower capacities for a 16-h charge. It is likely that some differences also exist, since the electrolyte-flooded electrode test environment is not the same as the cell environment. This may be particularly true for the charge efficiency, since the hydrogen electrode in the nickel hydrogen cell is extremely efficient in consuming oxygen. However, since both kinds of electrodes were tested under the same conditions, these test results point out real and significant differences in charge efficiency between the S/N 114 and Lot 1008 nickel electrodes.

The behavior of the S/N 114 electrodes during cycling was of interest, since extensive cycling of cells reportedly improved the cell capacity characteristics. An electrode sample from S/N 114 was subjected to 112 cycles, each cycle lasting 90 min and having approximately a 50% DOD at the C/2 rate. Charge return on each cycle was 104% of the capacity discharged, and a C/2 charge rate was used. The voltage characteristics during these cycles are indicated in Fig. 6. The largest voltage changes during the cycling are an initial drop followed by a gradual increase in the end-of-charge voltage. The cycling was found to have little effect on the high-discharge voltage characteristics or the degraded capacity characteristics (for a 16-h charge) for the S/N 114 electrode.

The impedance of the nickel electrodes during discharge was measured using the techniques described in Ref. 3. Starting from a fully charged state, the electrode capacity was discharged at a C/10 rate until the voltage fell to 0.2 V. Periodically during this discharge, the current was increased 10%, and the voltage response of the electrode was monitored as a function of time for 400 s, after which the current was returned to the C/10 rate. The voltage response as a function of time was used to calculate the impedance as a function of frequency, as has previously been described (Ref. 4). Following the C/10 discharge and a 1-h open circuit period, the electrode was discharged at C/100 until the voltage reached -0.5 V. During the C/100 discharge, the impedance was also periodically measured using the current step method, although the magnitude of the current step was adjusted under computer control to give a 3- to 5-mV voltage response in 400 s.

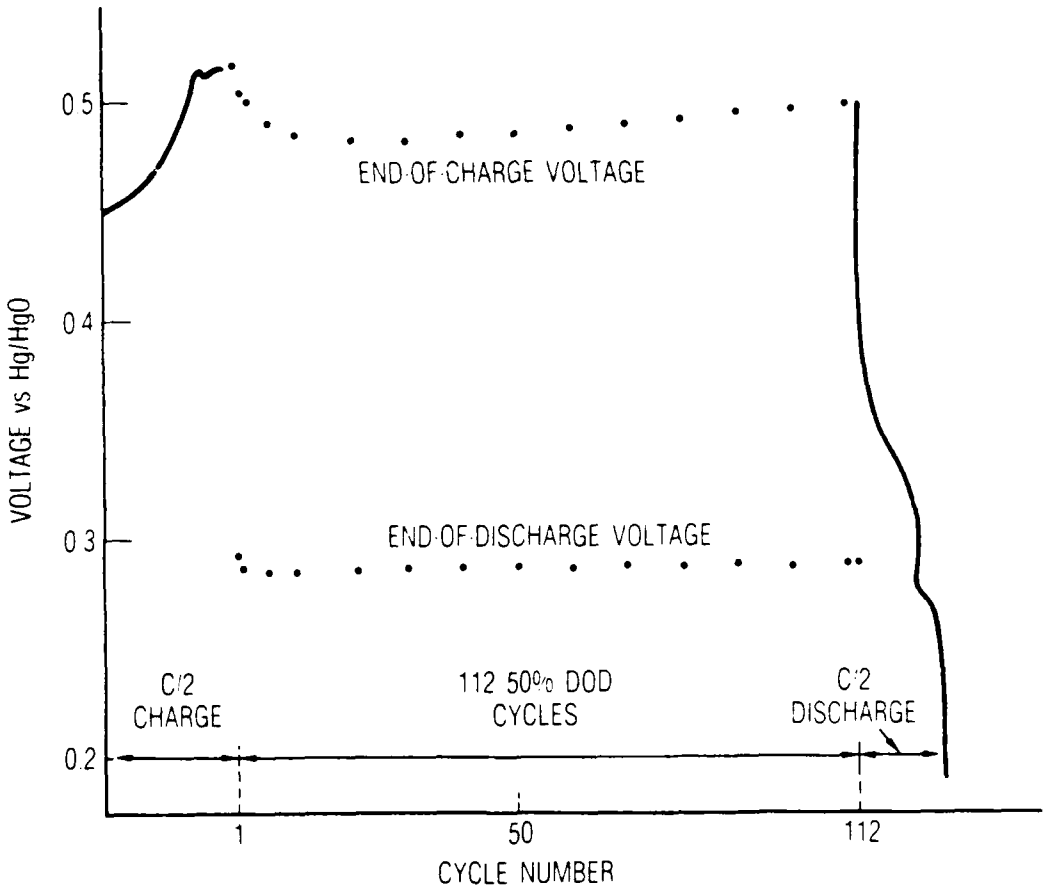

Fig. 6. Voltage During 112-Cycle Test of S/N 114 Ni Electrode

The electrode resistance, which is the low frequency limit approached by the impedance, is plotted as a function of electrode voltage in Fig. 7 for the Lot 1008 electrode, and for the S/N 114 electrode both before and after the 112-cycle test previously described. The principal difference in resistance between the two types of electrodes is again the offset in voltage seen in Fig. 7. This kind of voltage offset is similar to the effects reported in Ref. 3 that are caused by the addition of 5% cobalt or lithium to the nickel electrode. This observation, which is consistent with the previous observation of a higher discharge and charge voltage for the S/N 114 electrodes, suggested that detailed analyses for additives and/or contaminants should be performed.

A final electrical test involved measuring the I/V characteristics of the active material in the discharged state. This was done by discharging electrode samples to -0.5 V at a C/100 rate, after which the electrode was held at a constant voltage until a steady current was obtained. The I/V behavior thus obtained is indicated in Fig. 8. The I/V behavior indicated is not simple, and also is relatively similar for both types of electrodes except for a voltage offset. The behavior at currents above 0.04 mA/cm^2 results because the electrode state of charge was being depleted significantly during the measurement and the active material developed internal polarization from this process. While the S/N 114 electrodes appeared to have somewhat more residual capacity (probably from surface material that was not in close proximity to the current collector), this did not appear to be a major factor in the total capacity of these electrodes.

B. PHYSICAL ANALYSIS

Semiquantitative chemical analyses were performed by spark-arc techniques on bulk electrode samples that were ground up and had the current collector wires removed from the resulting powder. The pertinent results from these analyses are indicated in Table II.

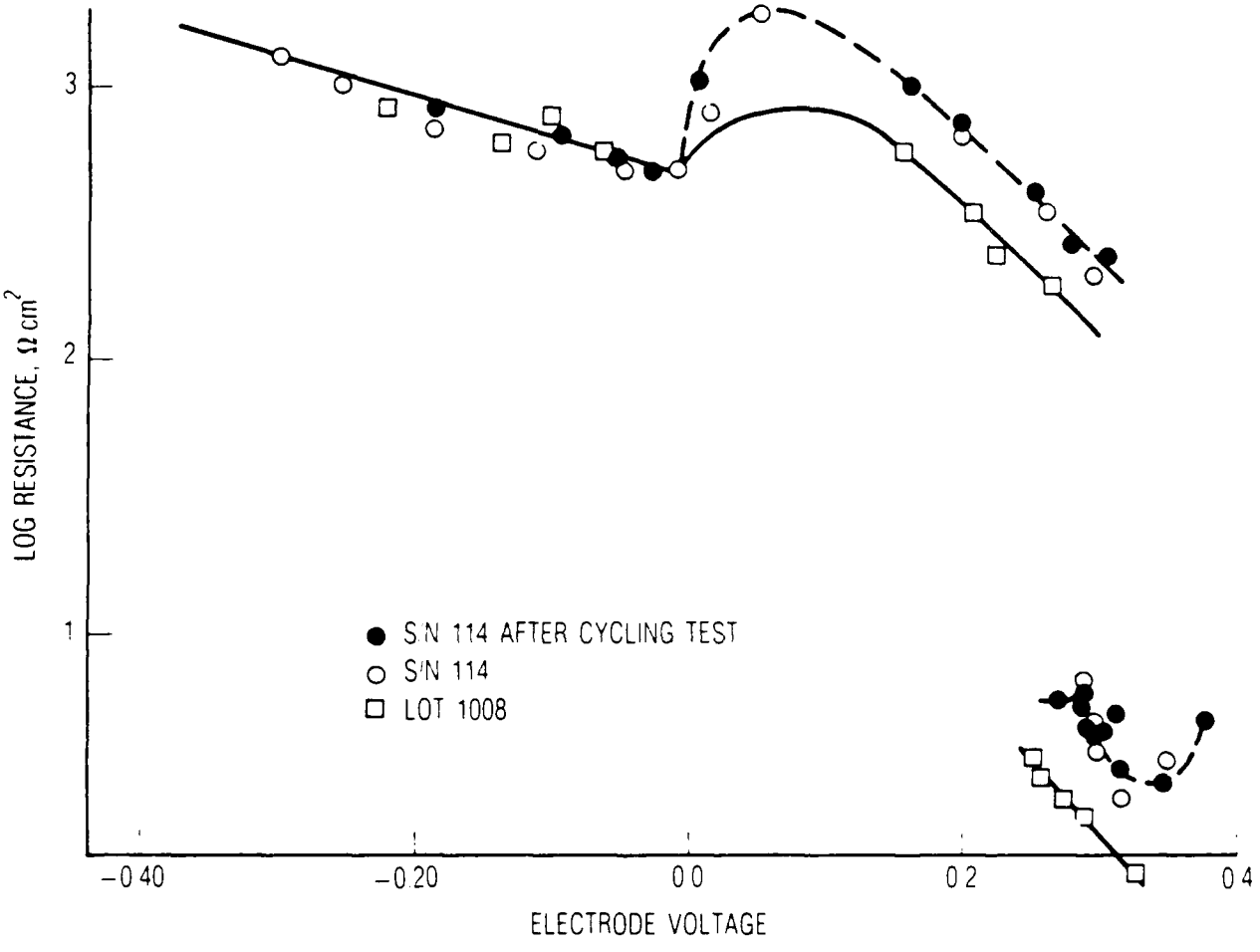

Fig. 7. Nickel Electrode Resistance During Discharge

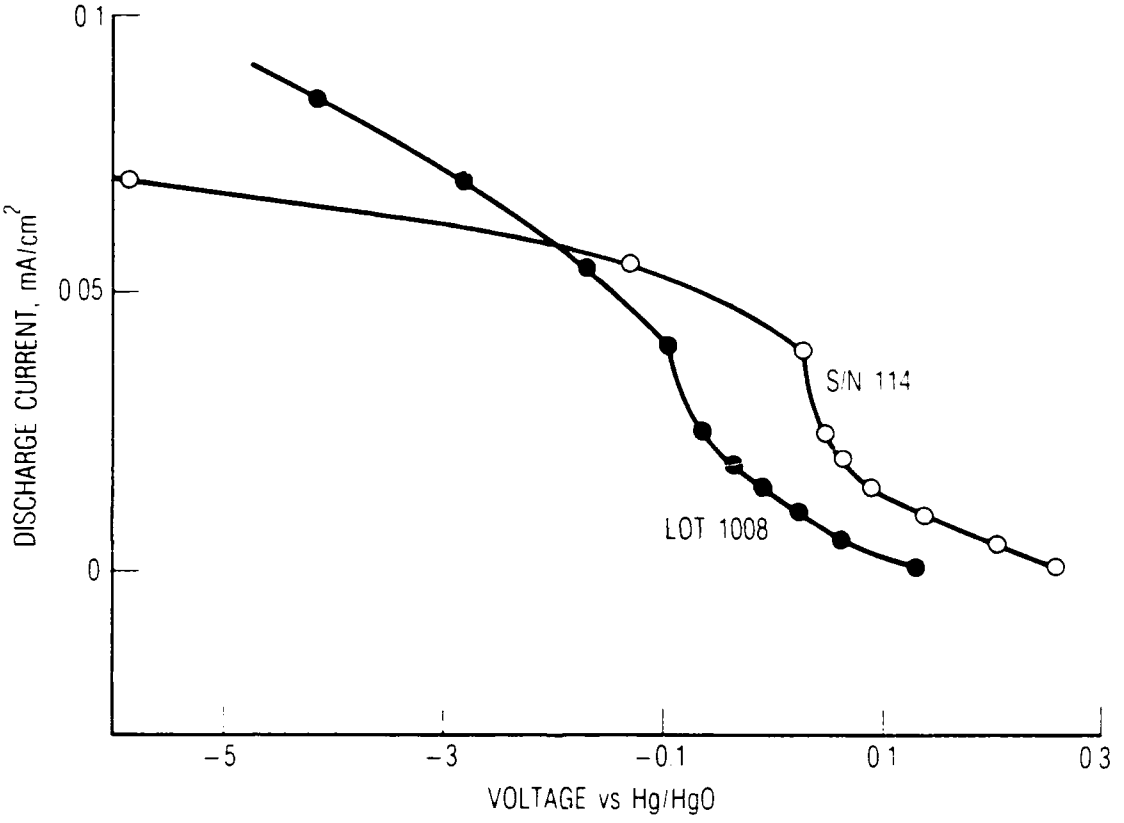

Fig. 8. I/V Characteristics of Discharged Ni Electrodes

Table II. Composition of Bulk Active Material/Sinter Powders

Component	S/N 114	Lot 1008
Ni metal	41.3%	40.4%
Nickel hydroxide	34.7	34.6
Cobalt hydroxide	2.3	3.2
Oxygen, hydrogen	remainder	remainder
Other metals	0.03	0.05

The ratio of cobalt to nickel hydroxides in these electrodes as nominally manufactured is 0.10. The results in Table II give 0.092 for this ratio for Lot 1008, and 0.066 for S/N 114. These results suggest that some depletion of cobalt in local areas may have occurred in the electrodes from the S/N 114 cell and, furthermore, that some mechanism may exist for cobalt movement. If this has occurred, then higher local concentrations of cobalt must be found elsewhere in the cell. If higher concentrations of cobalt cannot be found, then the reduced Co/Ni active material ratio may be due to corrosion of nickel metal to hydroxide during the cycling of the cell.

The structure of the active materials within the sintered electrodes was analyzed by x-ray diffraction studies of the powder obtained by grinding electrode samples at various states of charge after rinsing out the electrolyte and drying in vacuum. Figure 9 indicates the x-ray patterns obtained for the discharged electrodes. The patterns in Fig. 9 show the same peaks for both types of electrodes, a pattern that corresponds to nickel hydroxide. The Lot 1008 electrode has much broader peaks that are slightly shifted in position from the S/N 114 peaks. The lattice parameters for the active material are calculated from the peak positions, and are indicated in Table III for the two types of active material as well as for pure nickel hydroxide (Ref.5). Note that the peaks that go off scale in Fig.9 are due to the nickel metal in the powdered sinter.

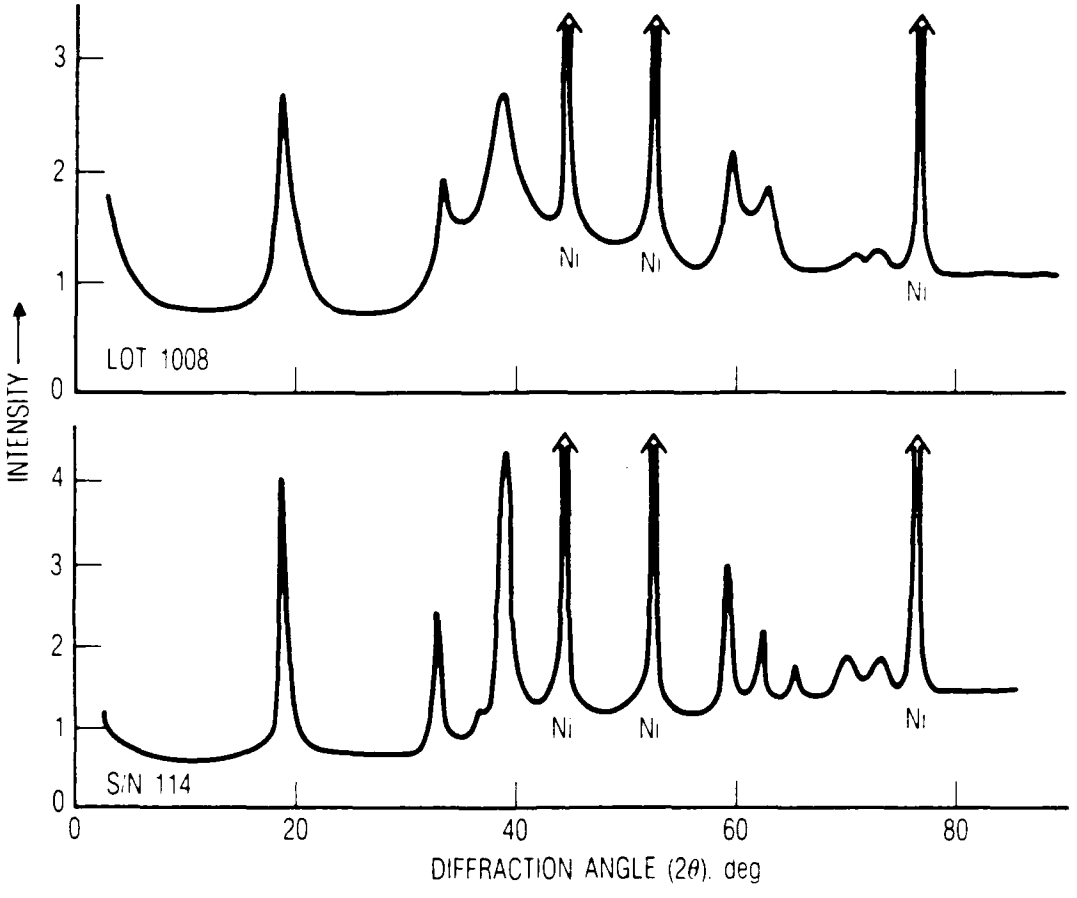

Fig. 9. X-Ray Diffraction Pattern for Discharged Electrodes

Table III. Lattice Parameters for Nickel Electrodes

Electrode	a(angstroms)	c(angstroms)
S/N 114	3.113	4.632
Lot 1008	3.078	4.620
Lot 1008,uncycled	3.057	4.373
Pure nickel hydroxide	3.126	4.605

The shift in lattice parameters in Table 3 from those of pure nickel hydroxide imply a distortion of the pure nickel hydroxide lattice, presumably by the presence of cobalt, the only additive. The large shift in lattice parameters for the uncycled Lot 1008 electrode, which had been stored for many years, probably reflects the formation of an inactive state, a process that has been observed to take place during long-term stand (Ref.6). The most noticeable difference seen in Fig. 9 for the two types of electrodes is the decrease in the width of the peaks for the S/N 114 electrode relative to the Lot 1008 electrode. Such peak narrowing was present in all comparisons between these electrode types, and may arise from reduced lattice strain, changes in stoichiometry, or from increased crystallite size. The only one of these possibilities that could cause a change in electrode voltage is a stoichiometry change. Therefore, the x-ray diffraction data appear to be most consistent with some kind of change in stoichiometry having occurred in the S/N 114 electrodes.

The results that have been described above indicate some significant changes in nickel electrodes that have been exposed to a reducing hydrogen environment in a nickel hydrogen cell for significant periods of time. The major changes are an increase (about 30 mV) in the charge, discharge, and open circuit voltages with concomitant reductions in charge efficiency, changes in the cobalt levels in the active material at a local (1 cm^2 sample) level, and a significant change in the stoichiometry of the active material. The S/N 114 electrodes also have important properties that remain unchanged from those of the unused Lot 1008 electrodes. The I/V characteristics in overcharge are not

altered greatly, indicating that the physical structure of the active material deposits has not been significantly degraded (Ref. 2). The impedance and I/V characteristics during discharge, as well as the dischargeable residual capacities, are also similar, indicating that reduced capacities are not likely to result from loss of active material contact with the current collectors or isolation of active material from discharge. The changes that have been found all suggest that some changes in the stoichiometry or chemical state of the active materials had occurred as a result of long-term exposure to a reducing environment. For this reason it was decided to initiate a detailed physical and chemical analysis of the changes that had occured in the active material.

B. EFFECTS OF OVERCHARGE AND REVERSAL ON ELECTRODE CHARACTERISTICS

In parallel with the preceding electrode characterization studies, some special tests were started in an effort to determine how the changes noted for the S/N 114 electrodes might be reversed, and to determine whether these same changes could be induced in Lot 1008 electrodes. Reversing the changes that were noted for the S/N 114 electrodes was attempted by two methods. The first involved the LEO-type cycling previously reported, and, for 112 cycles, was essentially unsuccessful in significantly modifying the electrode characteristics (the high discharge and recharge voltages).

The second method was to overcharge the electrode for extended periods of time, periodically testing an electrode sample for changes in voltage characteristics. This test involved 20 electrode samples (each 2 cm^2) from S/N 114 electrodes. Five samples each were put on charge at four different charge voltages; 0.43, 0.45, 0.47, and 0.49 V relative to a Hg/HgO reference electrode. The lowest voltage corresponds approximately to a C/100 trickle charge rate, and the highest voltage gave about a C/5 charge rate. Four of the five samples were removed over a 1- to 2-month period for testing, giving the results indicated in Table IV. These results indicate that no significant changes in voltage were obtained during the 1-month period. The fifth electrode was left on test for future evaluation, when this was felt to be appropriate.

Another test was done to try to induce the voltage characteristics observed in the S/N 114 electrodes in Lot 1008 electrode samples by subjecting samples to low-rate reversal for extended periods of time. Low-rate reversal generates hydrogen, maintaining a reducing environment and a high activity of hydrogen around the nickel electrode. Five Lot 1008 electrode samples were put in reversal at C/40, a rate that is not high enough to cause extensive damage to the electrode structure for long-term exposure. Four of these samples were removed over a 1- to 2-month period and tested, giving the results in Table IV. Some increase in voltage is seen after 1 week; however, at 1 and 2 months, the voltage had decreased. The decrease after the longer times of reversal was apparently due to an increase in electrode resistance due to the long-term reversal. Residual capacity also grew significantly, indicating some movement of active material. The fifth electrode was tested, as described later, in a manner that should eliminate the effects of changes in electrode resistance.

Table IV. Overcharge and Reversal Test Results

Electrode Treatment	Voltage at Midpoint of β-NiOOH Discharge Plateau				
	Initial	1 week	2 weeks	1 month	2 months
0.43 V charge	0.339	0.343	0.340	0.340	-----
0.45 V charge	0.336	0.345	0.343	0.340	-----
0.47 V charge	0.336	0.340	0.340	-----	0.340
0.49 V charge	0.337	0.340	0.340	-----	-----
C/40 reversal	0.285	0.300	0.272	-----	0.265

C. CHARACTERIZATION OF ACTIVE MATERIALS

Because of the previously presented results for the electrode tests, the active materials were analyzed, particularly for composition, stoichiometry, and uniformity. The chemical analysis for the electrodes suggested that some variability in cobalt levels existed, and that the cobalt, therefore, may be able to move under some conditions. Before doing a full-scale analysis, a

quick test was done to see if such cobalt movement was actually taking place. For the S/N 114 electrodes, a significant amount of active material had moved or oozed to the surface of the electrode during operation in the cell. Samples of this active material were scraped from the sinter surface to be analyzed for the relative amounts of nickel and cobalt. Because of the small amount of material in the sample, it was dissolved in 10% nitric acid, and the solution was analyzed by spark-arc techniques. After the nitric acid treatment, a small amount of brown colored material remained that was insoluble in the nitric acid. This insoluble material was also analyzed. The results of these analyses are indicated in Table V.

Table V. Chemical Analysis of S/N 114 Electrode Surface Material

Element	Acid Soluble Material	Insoluble Residue
Ni	89.8%	7.0%
Co	7.0	13.2
Zr	nil	21.7
Y	nil	50.4
Si	0.9	2.4
Fe	0.6	2.5
Mg	0.2	0.4
Mn	0.2	<0.3
Al	0.1	1.2
Cu	0.1	0.1
Na	0.5	nil
Ti	0.1	0.6
Ca	0.1	0.5
Cd	0.2	nil

The results in Table 5 suggest that significant concentration of the cobalt in the S/N 114 electrode has taken place and that, furthermore, under some conditions the material containing enhanced levels of cobalt is insoluble

in nitric acid. This may provide a convenient way of detecting the movement of cobalt from its normal sites in the nickel hydroxide lattice. The large amounts of zirconium and yttrium listed as insoluble residue in Table V are due to zircar fibers that were lodged in the surface of the electrode (zircar is the separator in these cells). These results provided an approach used for a more detailed analysis of the active material. Further analysis was done on four samples of active material. Sample 1 was prepared by overcharging a S/N 114 electrode at the C/5 rate for 24 h, a procedure that caused a large amount of surface active material to be thrown from the electrode into the 31% KOH electrolyte. The material thrown from the electrode was filtered, magnetically treated to remove any sinter particles, washed with deionized water and dried. The dried powder was labeled Sample 1. Sample 2 was prepared by powdering a piece of discharged S/N 114 electrode as obtained from the cell, following rinsing and drying. After removal of the wires from the nickel screen, the powder was treated with a plastic coated magnet while in an aqueous slurry until all sinter particles were removed. The powder remaining after filtering and drying was labeled Sample 2. Samples 3 and 4 were prepared in the same way as Sample 2, except that pieces of Lot 1008 electrode as bagged by the factory (nearly discharged) were used for Sample 3, and a fully charged piece was used for Sample 4.

Samples of the powdered active material were prepared for ESCA and SEM analyses by rubbing the powder into the surface of a piece of indium foil, which provided a conductive matrix that would not interfere with the analyses. ESCA analysis, which can detect cobalt or nickel levels down to only 15 to 20% for this type of sample, was only able to detect cobalt in Samples 2 and 4, which were both generated by charging the electrodes. The ESCA analyzes a surface layer on the active material particles that is only 15 to 20 Å thick. Samples 2 and 4 both contained about half as much cobalt as nickel in this surface layer, or a cobalt to nickel ratio of 0.5. Potassium was only found in the fully charged sample from Lot 1008, Sample 4, indicating that the active material had been converted significantly to γ-NiOOH in the surface layer of this sample. These results clearly indicate that a mechanism exists for concentrating the cobalt levels at the active material/electrolyte interface,

and that the mechanism for producing cobalt-rich hydroxides or oxides involves oxidation, or charging of the active material.

X-ray diffraction measurements of the four powder samples gave the results indicated in Figs. 10 and 11. These x-ray diffraction results for the active materials are for the most part similar to those previously obtained for the electrodes during the electrode characterization testing, except that the peaks due to nickel metal have been eliminated. Sample 1 shows the x-ray pattern for nickel hydroxide. Sample 2 is a mixture of the nickel hydroxide and a small amount of γ-NiOOH. Sample 2 also contains significant quantities of zircar fibers, as indicated by the peak at about 30 deg. Sample 3 has the nickel hydroxide structure; however, it is quite disordered as indicated by the broad peaks. Sample 4, although having somewhat broadened peaks, basically shows the γ-NiOOH structure that is characteristic of fully charged active material.

SEM study of these four samples revealed active material particles from 0.5 to 5 μm in size for all samples. Elemental analysis was obtained using the energy dispersive x-ray capability of the SEM instrument. This analysis was done for each sample as a whole, as well as for several small active material particles less than 1 μm in diameter. This analysis technique examines the composition about 1.5 μm into the material, thus it is essentially a bulk analysis method for particles less than 1 μm in diameter. The results of these analyses are indicated in Table VI. The results in Table VI show cobalt level enhancements over the 10% added to the bulk active material during manufacturing. This appears to be a surface effect on the particles of active material, and is particularly noticeable for Samples 1 and 2 where cobalt levels ranged between about 20 and 31%. These results, when considered with the previous ESCA results, suggest that the cobalt level is undergoing enhancement by some process in a layer of active material grains near the surface of the particles. The thickness of the affected layer is significantly greater for S/N 114 active material than for Lot 1008 active material.

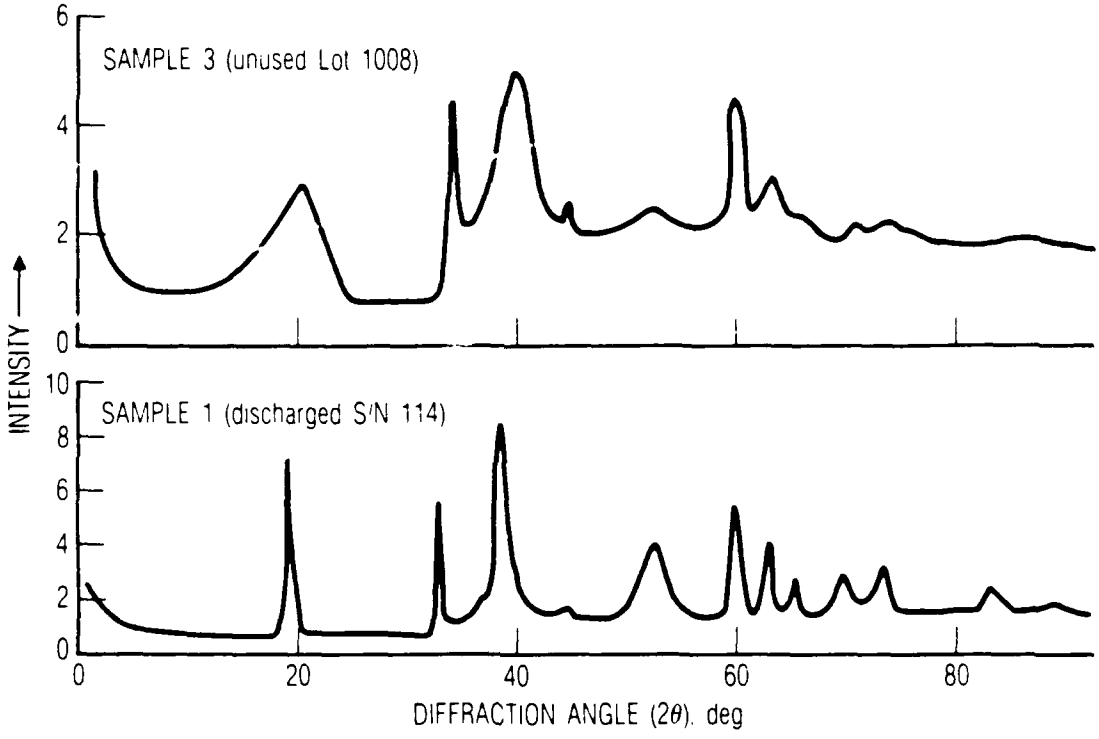

Fig. 10. X-Ray Diffraction Patterns for Ni Active Material Samples from Electrodes Prior to Electrical Activity

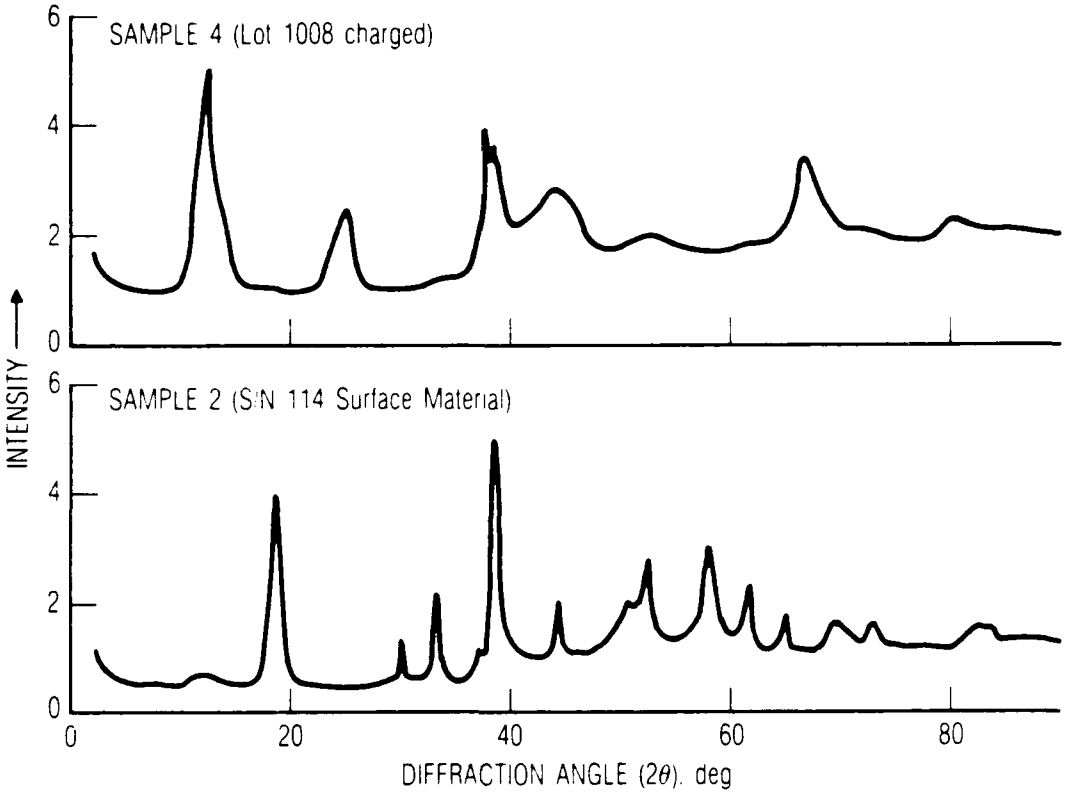

Fig. 11. X-Ray Diffraction Patterns for Ni Active Material Samples Prepared by Charging.

Table VI. Cobalt and Nickel Analyses from SEM Studies

	Sample 1	Sample 2	Sample 3	Sample 4
Overall:				
Ni	83.2%	81.7	88.1	86.6
Co	16.8	18.3	11.9	13.4
Co/Ni	0.202	0.224	0.135	0.155
Single Particle:				
Ni	83.2	76.1	85.7	86.0
Co	16.8	23.9	14.3	14.0
Ni/Co	0.202	0.314	0.167	0.163

From Table VI the thickness of the layer having enhanced cobalt levels appears to be on the order of 1 μm or less for S/N 114 active material, and appears more prominently in the partially charged surface material (Sample 2).

A bulk chemical analysis for relative amounts of nickel and cobalt was done on the four samples by dissolving them in 10% nitric acid. To guarantee dissolution of all soluble material, this step was done by twice heating the nitric acid mix to boiling, since for Samples 1 and 2 a residue remained that appeared insoluble in the acid. The dissolved solutions were submitted for spark-arc analysis along with the insoluble residue from Sample 1. The amount of insoluble residue from Sample 2 was insufficient for a good bulk analysis, and, therefore, was prepared on indium foil for elemental analysis using the SEM. Part of the insoluble residue from Sample 1 was also prepared for SEM analysis in a similar manner.

The SEM analysis of the insoluble residue from Sample 2 showed large amounts of zircar fiber particles, significant quantities of platinum catalyst particles, and small amounts of cobalt associated with the zircar fibers. In addition, some masses of material were found which contained high levels of iron. These results clearly indicate that, in these nickel hydrogen cells, significant quantities of platinum particles find their way to the nickel electrode, presumably as a result of popping holes through the zircar, which occurs during overcharge as gases recombine rapidly. The SEM analysis of the Sample 1 insoluble residue indicated that the bulk of the insoluble material had a composition of about 80 to 90% cobalt and 10 to 20% nickel. There was some evidence again for zircar and platinum, although these were much less of the total material than for the Sample 2 residue. These results indicate that some process is operative that converts the mixed nickel/cobalt hydroxide into an almost pure cobalt oxyhydroxide or oxide that is insoluble in acid in the totally discharged state that is achieved by shorting down a nickel hydrogen cell for several weeks. X-ray diffraction studies of the insoluble residue from Sample 1 showed the nickel hydroxide structure only, indicating that the 80 to 90% cobalt material that was isolated is either amorphous (probably because of small particle size), or that it remains in the nickel hydroxide structure. It should be pointed out that the nickel hydroxide and cobalt hydroxide structures are similar enough that either could exist as a distorted version of the other structure in a mixed system.

Chemical analyses of the dissolved sample materials are presented in Table VII for cobalt and nickel, which were the principal elements other than oxygen and hydrogen, which account for nearly all the material that was not nickel or cobalt.

The analyses of Table VII appear to have a systematic enhancement of cobalt in all the first four samples over the amount expected based on the previous bulk analyses for the electrodes (Table II). This cobalt enhancement is likely to arise during the magnetic separation of the active material from the powdered sinter. The powdered sinter retains active material that is stuck to it, and if the material thus retained is lower in cobalt, a net cobalt enhancement will be observed in the separated material. In spite of this

Table VII. Semiquantitative Analysis of Active Material Samples

Sample	Nickel	Cobalt
(1) S/N 114 discharged	54.2%	9.3%
(2) S/N 114 surface,charged	52.3	11.2
(3) Lot 1008 discharged	54.2	9.3
(4) Lot 1008 charged	54.4	9.1
Sample 1, insoluble residue	6.0	57.5

uncertainty the results in Table VII indicate that, although significant quantities of insoluble cobalt-rich material are present in the S/N 114 active material, a large amount of the cobalt is retained in an acid soluble form in the active material. It is not clear from these analyses whether the cobalt that is retained in the soluble active material remains as desired in the active material structure, or whether it exists as another inactive phase that was undetected in the x-ray diffraction studies.

D. HYPOTHESIS FOR COBALT SEGREGATION MECHANISM

The results that have been presented indicate that cobalt is segregating from the uniformly mixed active material deposit produced during initial electrode fabrication. The segregation produces several phases. One is a somewhat cobalt-depleted active material and another is a high-cobalt-content oxide or hydroxide. Other phases may exist; however, these two are the minimum required to account for the results that have been obtained. The mechanism for cobalt segregation is likely to involve several steps, including lengthy exposure to a reducing environment followed by oxidation of the materials generated in the reducing environment. A number of reactions that involve the constituents of the nickel electrode and that can occur at reducing voltages have been documented (Ref. 7), and are listed here along with the voltage at which each reaction occurs relative to the Hg/HgO reference electrode.

$$Co + 2OH^- \rightleftharpoons 2e^- + Co(OH)_2 \qquad -0.83\ V \qquad (2)$$

$$Ni + 2OH^- \rightleftharpoons 2e^- + Ni(OH)_2 \qquad -0.82\ V \qquad (3)$$

$$Co + CO_3^{--} \rightleftharpoons 2e^- + CoCO_3 \qquad -0.74\ V \qquad (4)$$

$$Ni + CO_3^{--} \rightleftharpoons 2e- + NiCO_3 \qquad -0.55\ V \qquad (5)$$

$$Pt + 2OH^- \rightleftharpoons 2e^- + Pt(OH)^2 \qquad +0.05\ V \qquad (6)$$

$$Co(OH)_2 + OH^- \rightleftharpoons Co(OH)_3 + e^- \qquad +0.07\ V \qquad (7)$$

$$Ni(OH)_2 + OH^- \rightleftharpoons NiOOH + H_2O + e^- \qquad +0.38\ V \qquad (8)$$

The last of these reactions, reaction (8), is the one normally regarded to occur in nickel electrodes. The voltage of reaction (8), and probably those of the other cobalt and nickel reactions as well, will be changed somewhat by the presence of mixed cobalt/nickel compounds. All of the other reactions can occur in the opposite direction as written above when the nickel electrode is brought down to a low voltage, and may occur as written when the nickel electrode is charged. The reaction involving platinum requires that platinum be present in the nickel electrode, which was the case for the S/N 114 electrodes. Since carbonates are always present in alkaline electrolyte, probably more so in the laboratory studies reported here than in the actual nickel hydrogen cells, the reactions of the metal carbonates are also shown. In the nickel electrode, all the reactions indicated above except the last two may be quite slow, particularly when insufficient conductivity exists in the active material to pass much current.

A relatively straightforward mechanism that gives segregation of cobalt involves reactions (2) and (3), which should give slow reduction of nickel/cobalt hydroxides to particles of nickel and cobalt metal when the nickel electrode is held at low voltages. When excess hydrogen is present in the nickel hydrogen cell, the capacity that this hydrogen provides, coupled

with the catalytic activity of the nickel metal in the electrode, will drive these reactions. The reaction rates are expected to be slow, and should be strongly dependent on the quality of contact of the active material with the sinter and between the grains of active material. The presence of platinum may accelerate these reactions because of the high surface area and catalytic activity of the platinum.

Small particles of nickel and cobalt metal formed by the reverse of reactions (2) and (3) at low voltages will be readily oxidized when the voltage is increased during electrode charging. The metals will first oxidize to the hydroxides. The cobalt hydroxide particles thus formed will be further oxidized to a trivalent cobalt hydroxide by reaction (7) just above zero volts vs Hg/HgO. The platinum surfaces will also be oxidized by reaction (6), which is likely to passivate much of the Pt catalytic activity and prevent it from affecting the normal operating characteristics of the electrode. The trivalent cobalt produced by reaction (7) is soluble in the alkaline electrolyte. The dissolved cobalt ions will either be incorporated back into the active material structure or will precipitate as an insoluble cobalt oxide/hydroxide (perhaps Co_3O_4 or CoO_2) on the active material and metal surfaces exposed to the electrolyte. At present it is not known how much cobalt is reincorporated into the active material relative to the amount precipitated. The precipitated cobalt compounds are inert to any further changes.

E. TEST FOR PROPOSED COBALT SEGREGATION MODEL

To determine whether the model described above for cobalt segregation is consistent with electrode performance, the following tests were done to directly monitor reactions (2) through (8). The fifth Lot 1008 electrode sample that was reversed at C/40 for 2 months was used in this test. Since this electrode had been held for 2 months in a highly reducing environment, it should contain evidence for the reduction products from reactions (2) through (8). These reactions were detected by EVS (electrochemical voltage spectroscopy) on this electrode. The EVS technique sweeps the electrode voltage through a region where reactions of interest can occur, with the sweep

rate being controlled so that it is slower than the rate at which the reactions of interest occur. This technique provides a plot of dQ/dV (the density of reactive sites) as a function of potential. Using computer control, EVS is well suited to detecting and characterizing extremely slow electrochemical reactions.

The Lot 1008 electrode that was reversed for 2 months was run through an EVS scan from the hydrogen evolution region (about -1.0 V) up to 0.5 V, where it is in a nearly fully charged state. A sweep rate of 0.01 mV/sec was used. The results are indicated in Fig. 12. Figure 12 does indeed show several of the reactions of interest. A double peak between -0.8 and -0.7 V is consistent with oxidation of cobalt and nickel metal per reactions (2) and (3). The peak at about 0.05 V is consistent with oxidation of cobalt hydroxide to trivalent cobalt. Thus the scan in Fig.12 is consistent with the model outlined above for cobalt segregation.

Following this scan, the electrode was put through several charge-discharge cycles, during which none of the peaks except the one at 0.45 V (normal electrode charging) was seen again. This supports the contention that the reactions causing these peaks are quite slow. Following the cycling, the electrode was removed from the plastic cell, and when examined was found to have a very thin brown film deposited on the shiny nickel metal tab that was attached to the electrode. ESCA analysis of the brown film indicated that it was a cobalt oxide that was not divalent or trivalent. This observation suggests that the film is a cobalt oxide or hydroxide precipitated from the trivalent cobalt species in solution, which are unstable at the electrode charging potentials (Ref.6).

Several tests were done to study factors that may influence the rate at which cobalt segregation reactions can occur. The first of these started with an uncycled Lot 1008 electrode sample. This electrode was dipped several times in a suspension of platinum black in acetone in an attempt to put platinum into the active material. After drying, the electrode was reversed at C/10 for 5 days, after which an EVS scan was done. The results are shown in Fig. 13. Only two small peaks are present at lower potentials in Fig. 13.

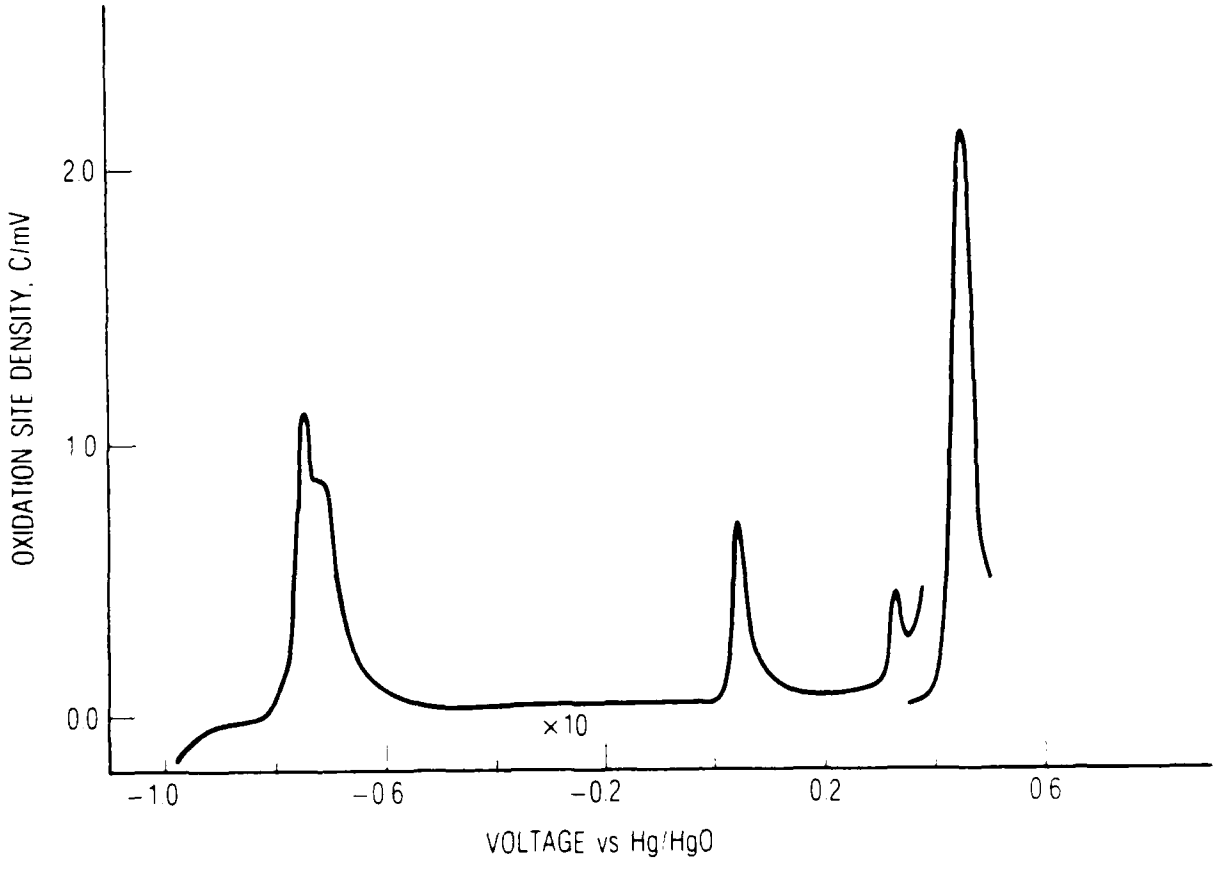

Fig. 12. EVS Scan of Lot 1008 Electrode Reversed for 2 Months at C/40. Scan is from initial rest voltage to 0.5 V, at 0.02 mV/sec.

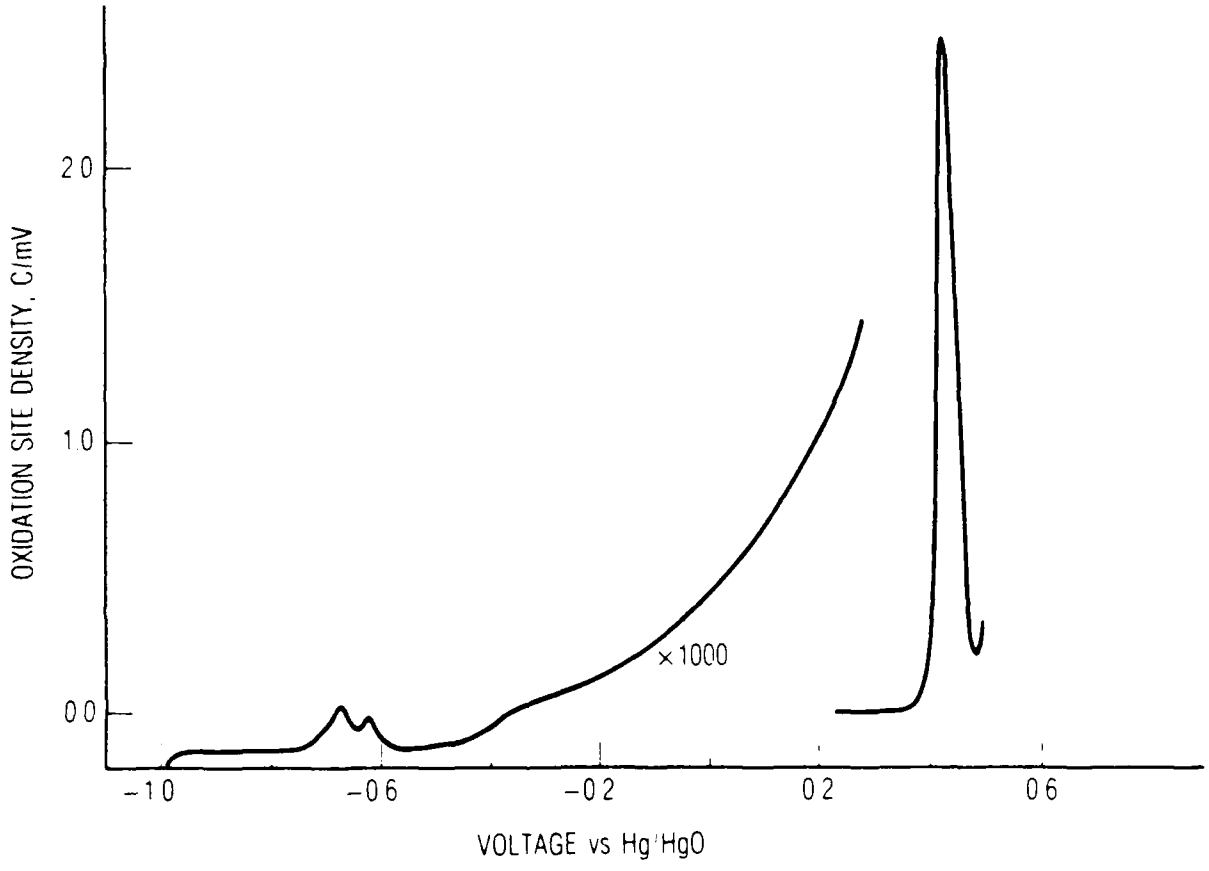

Fig. 13. EVS Scan for Lot 1008 Electrode Reversed for 5 Days at c/10, after Dipping in Pt Suspension. Scan is from rest potential to 0.5 V, at 0.01 mV/sec.

These results suggest that essentially no cobalt segregation took place over this 5-day period. Since it is not clear that the platinum was in intimate contact with much of the active material, the interpretation of these results is somewhat uncertain.

A similar test used a piece of S/N 114 electrode that had also been in reversal for 5 days at C/10, providing the EVS results in Fig. 14. This scan shows a large peak due to nickel and cobalt metal oxidation (-0.8 V), two smaller peaks near -0.7 and -0.6 V that may be from the carbonate reactions (reactions 4 and 5), and a large peak at 0.05 V corresponding to formation of trivalent cobalt. These results indicate that, in the S/N 114 electrodes, conditions are such that cobalt segregation reactions can occur much more rapidly than for Lot 1008 electrodes. These tests do not answer the question of how much platinum accelerates the rate of cobalt segregation, since for S/N 114 electrodes that are known to have Pt in intimate contact with the active material, high reaction rates are observed. For Lot 1008, a low rate for the cobalt segregation reactions was observed, but the Pt may not have been adequately imbedded in the active material. Another possibility, explaining the differences in reaction rates implied by Figs. 13 and 14, is simply that the morphology and contact area with catalytic surfaces differ significantly for the two different types of electrodes.

The EVS data can be used to obtain a precise measure of the shifts in characteristic voltages that have been observed to accompany the changes in performance of the S/N 114 electrodes. Table VIII indicates the EVS peak positions for the normal electrode charge/discharge process, nominally reaction (8).

Table VIII. EVS Peak Voltages for Reaction (8)

Electrode	Peak Charge	Peak Discharge
S/N 114	0.462, 0.485 V	0.339 V
Lot 1008, 5-day reversal	0.424	0.284
Lot 1008, 2-month reversal	0.427	0.300

The results in Table VIII show that discharge voltage characteristics are the most sensitive measure of removal of cobalt from the active material lattice, since a 55-mV difference in discharge voltage peaks is obtained for S/N 114 relative to Lot 1008. The results of Table VIII also suggest that roughly 25% of the cobalt segregation in S/N 114 active material was induced in the Lot 1008 electrode by 2 months of reversal hydrogen enviroment.

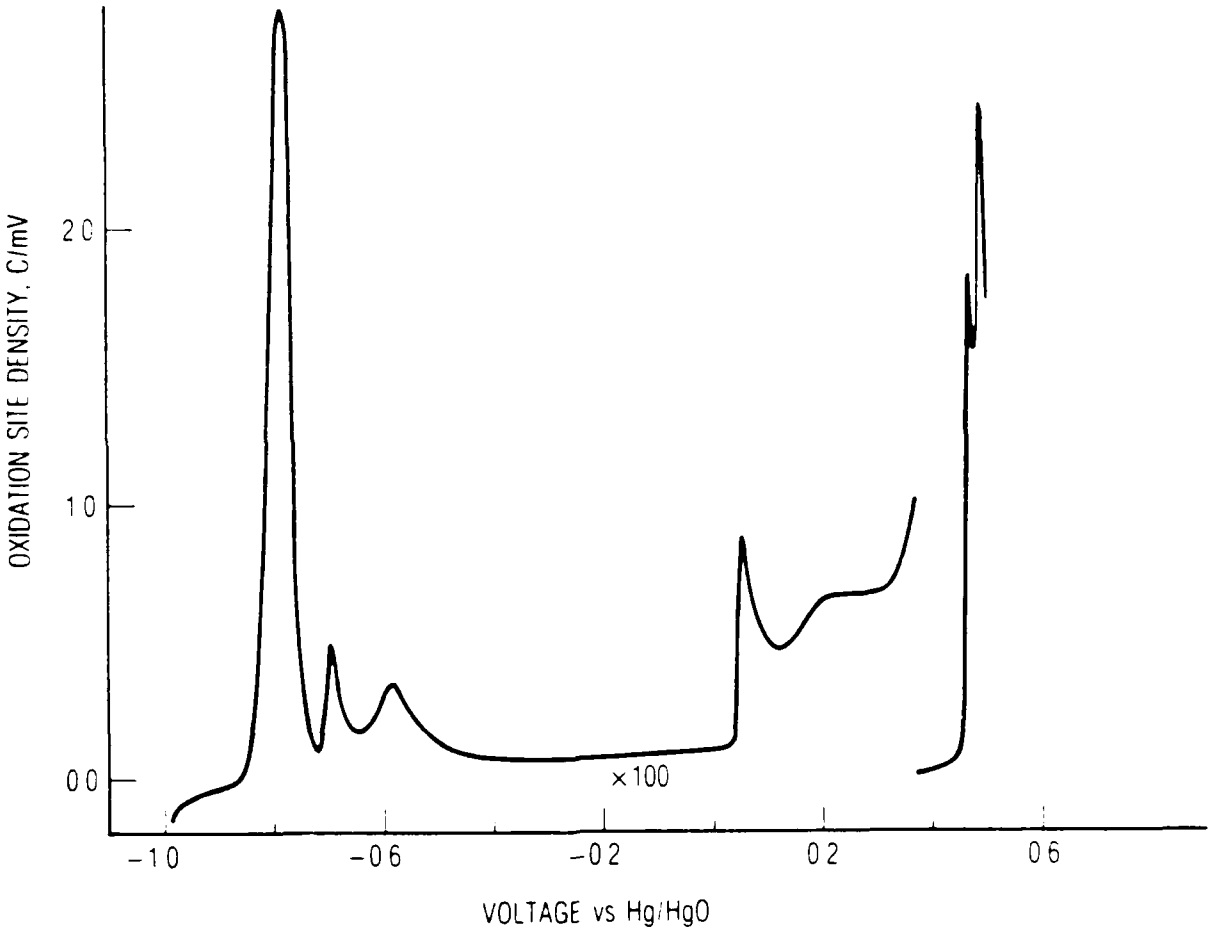

Fig. 14. EVS Scan for S/N 114 Electrode Reversed for 5 Days at C/10. Scan is from rest potential to 0.5 V, at 0.01 mV/sec.

III. CONCLUSIONS

1. The charge efficiency of the nickel electrodes from a cycled cell is significantly reduced relative to an unused electrode. This may be at least partly due to normal changes resulting from the cycling experienced by the cell.

2. Significant segregation of cobalt has occurred in the nickel electrodes from the cycled NiH_2 cell. As much as 30 to 50% of the cobalt that was initially incorporated into the active material structure has been converted to a cobalt-rich material having no electrochemical activity. The depletion of cobalt additive is likely to occur primarily in the active material adjoining the surfaces of the nickel sinter and, therefore, may cause a more significant impact on performance than if the cobalt were uniformly depleted throughout the active region.

3. A process has been identified that is likely to have been responsible for the cobalt segregation. This segregation process is much more rapid in electrodes from the NiH_2 cell than in unused electrodes. Platinum contamination in the nickel electrodes of the cell may contribute to the higher reaction rates for the segregation process.

4. The cobalt segregation is expected to change the characteristics of the nickel electrodes in the following ways:

   - An inactive cobalt-rich material will build up; removing some active capacity, altering positive/negative charge balance, and possibly isolating some active material from discharge.

   - Both charge and discharge voltages will tend to be increased.

   - Charge efficiency will be reduced (direct consequence of increased charging voltage).

   - Reduction in the amount of cobalt in the active material lattice may increase the stress levels that charge/discharge operation exerts on active material and sinter structures over long-term operation.

5. Cobalt segregation can occur only when the nickel electrode is held at or near the hydrogen electrode voltage, which can happen during cell short-down or stand when excess hydrogen is present. The rate of cobalt segregation processes appears to be highly variable, depending on factors that are not fully understood at present.

6. The processes leading to cobalt segregation are stopped if the nickel electrode voltage is kept well above the hydrogen voltage.

REFERENCES

1. R. Barnard, G. T. Crickmore, J. A. Lee, and F. L. Tye, J. Applied Electrochem. 10, 61 (1980).

2. A. H. Zimmerman and P. K. Effa, Extended Abstracts of the Fall Meeting of the Electrochemical Society, Vol. 84-2, The Electrochemical Society, Inc., 1984.

3. A. H. Zimmerman and P. K. Effa, Proc. of the 19th IECEC, 1984, p. 169.

4. A. H. Zimmerman, M. R. Martinelli, M. C. Janecki, and C. C. Badcock, J. Electrochem. Soc. 129, 289 (1982).

5. Powder Diffraction File, JCPDS International Center for Diffraction Data, 1983, File 14-117.

6. R. Barnard, C. F. Randell, and F. L. Tye, Power Sources 8, 401 (1981).

7. M. S. Antelman, The Encyclopedia of Chemical Electrode Potentials, Plenum Press, New York, 1982.

8. M. Pourbaix, Atlas of Electrochemical Equilibria in Aqueous Solutions, second edition, National Assoc. of Corrosion Engineers, 1974, pp.323-325.

LABORATORY OPERATIONS

The Aerospace Corporation functions as an "architect-engineer" for national security projects, specializing in advanced military space systems. Providing research support, the corporation's Laboratory Operations conducts experimental and theoretical investigations that focus on the application of scientific and technical advances to such systems. Vital to the success of these investigations is the technical staff's wide-ranging expertise and its ability to stay current with new developments. This expertise is enhanced by a research program aimed at dealing with the many problems associated with rapidly evolving space systems. Contributing their capabilities to the research effort are these individual laboratories:

Aerophysics Laboratory: Launch vehicle and reentry fluid mechanics, heat transfer and flight dynamics; chemical and electric propulsion, propellant chemistry, chemical dynamics, environmental chemistry, trace detection; spacecraft structural mechanics, contamination, thermal and structural control; high temperature thermomechanics, gas kinetics and radiation; cw and pulsed chemical and excimer laser development including chemical kinetics, spectroscopy, optical resonators, beam control, atmospheric propagation, laser effects and countermeasures.

Chemistry and Physics Laboratory: Atmospheric chemical reactions, atmospheric optics, light scattering, state-specific chemical reactions and radiative signatures of missile plumes, sensor out-of-field-of-view rejection, applied laser spectroscopy, laser chemistry, laser optoelectronics, solar cell physics, battery electrochemistry, space vacuum and radiation effects on materials, lubrication and surface phenomena, thermionic emission, photosensitive materials and detectors, atomic frequency standards, and environmental chemistry.

Computer Science Laboratory: Program verification, program translation, performance-sensitive system design, distributed architectures for spaceborne computers, fault-tolerant computer systems, artificial intelligence, microelectronics applications, communication protocols, and computer security.

Electronics Research Laboratory: Microelectronics, solid-state device physics, compound semiconductors, radiation hardening; electro-optics, quantum electronics, solid-state lasers, optical propagation and communications; microwave semiconductor devices, microwave/millimeter wave measurements, diagnostics and radiometry, microwave/millimeter wave thermionic devices; atomic time and frequency standards; antennas, rf systems, electromagnetic propagation phenomena, space communication systems.

Materials Sciences Laboratory: Development of new materials: metals, alloys, ceramics, polymers and their composites, and new forms of carbon; nondestructive evaluation, component failure analysis and reliability; fracture mechanics and stress corrosion; analysis and evaluation of materials at cryogenic and elevated temperatures as well as in space and enemy-induced environments.

Space Sciences Laboratory: Magnetospheric, auroral and cosmic ray physics, wave-particle interactions, magnetospheric plasma waves; atmospheric and ionospheric physics, density and composition of the upper atmosphere, remote sensing using atmospheric radiation; solar physics, infrared astronomy, infrared signature analysis; effects of solar activity, magnetic storms and nuclear explosions on the earth's atmosphere, ionosphere and magnetosphere; effects of electromagnetic and particulate radiations on space systems; space instrumentation.

END

DATE

FILMED

DTIC

6-88